Aerosol and Air Quality Research, 15: 2246–2257, 2015

ISSN: 1680-8584 print / 2071-1409 online
doi: 10.4209/aaqr.2014.12.0321

Secondary Formation of Sulfate and Nitrate during a Haze Episode in Megacity Beijing, China

Xingang Liu[1*], Kang Sun[2], Yu Qu[3], Min Hu[2], Yele Sun[3], Fang Zhang[4], Yuanhang Zhang[2*]

[1] *State Key Laboratory of Water Environment Simulation, School of Environment, Beijing Normal University, Beijing 100875, China*
[2] *State Key Joint Laboratory of Environment Simulation and Pollution Control, College of Environmental Sciences and Engineering, Peking University, Beijing 100871, China*
[3] *State Key Laboratory of Atmospheric Boundary Layer Physics and Atmospheric Chemistry, Institute of Atmospheric Physics, Chinese Academy of Sciences, 100029, China*
[4] *College of Global Change and Earth System Science, Beijing Normal University, Beijing 100875, China*

ABSTRACT

A heavy haze episode that occurred in Beijing from 20 September to 27 September, 2011 was observed to explore the secondary processes of the haze episode. During the haze episode, the relatively stable synoptic conditions and regional transport from polluted areas in the south and southwest of Beijing favored the formation of haze. Significant increases of $PM_{2.5}/PM_{10}$ ratio was observed during haze period, which implied that the haze was caused by fine particles. Additionally, the presence of secondary inorganic pollutants (SO_4^{2-}, NO_3^- and NH_4^+) sharply increased during the haze episode, which indicated that secondary processes significantly strengthened the haze episode. The sulfur oxidation ratio (SOR) sharply increased from a non-haze episode with a highest value of 0.11 to a haze episode with a highest value of 0.62. Low correlations between SOR and O_3 and the temperature were found, whereas a high correlation between SOR and RH was found during the haze episode, which implied that sulfate was mainly produced by the aqueous-phase oxidation of SO_2 rather than the gas-phase conversion of SO_2 to sulfate in haze episode in Beijing. Furthermore, a fine linear relationship between SOR and the surface area (dS) of particles smaller than 1 μm confirmed the heterogeneous processes of sulfate formation in haze episode. The nitrogen oxidation ratio (NOR) also sharply increased from a non-haze episode with a highest value of 0.03 to a haze episode with a highest value of 0.26, which indicated more intense secondary formation of nitrate in haze episode. Nitrate was found to be mainly produced by a homogenous reaction under ammonium-rich conditions. Higher RH in haze episode reduced the thermodynamic equilibrium constant Ke', and favored the thermodynamic equilibrium reaction of $HNO_3(g) + NH_3(g) \leftrightarrow NH_4NO_3(s, aq)$ to formed nitrate, which might help explain the enhanced homogenous production of nitrate in haze episode. In addition, a good empirical fit ($R^2 = 0.70$) between NOR and dS was found, which indicated that the particle surface area significantly contributed to the intense homogeneous production of nitrate in haze episode.

Keywords: Haze; SOR; NOR; Secondary formation mechanism; Beijing.

INTRODUCTION

Air pollution has become a serious problem in China with the rapid development of the economy, increased population and urbanization. Among these problems, haze has received significant domestic and overseas attention because many cities in China have suffered from heavy haze pollution in recent years, such as the serious haze episode that broke the records over the past 60 years occurred in Beijing on 12–13 January, 2013 (highest hourly $PM_{2.5}$ concentration of 886 μg m^{-3}, http://www.nasa.gov/multimedia/imagegallery/image_feature_2425.html). Haze is defined as the condition when the daily average relative humidity is less than 90%, and the daily average visibility is less than 10 km, excluding precipitation, snow and dust storms (Wu *et al.*, 2005). Haze is an atmospheric phenomenon with smoke, dust and moisture suspended in the air and impairing visibility (Watson *et al.*, 2002). Haze can not only reduce visibility and affect traffic safety, but it also has detrimental effects on human health; for example, it causes respiratory and cardiovascular diseases (Tie *et al.*, 2009). Therefore, it

* Corresponding author.
Tel.: + 86-10-58805218
E-mail address: liuxingang@bnu.edu.cn (Xingang Liu); yhzhang@pku.edu.cn (Yuanhang Zhang)

is important to understand the formation mechanism of haze in China, to implement control measures and help residents avoid impairment from haze.

Previous studies have found that haze is characterized by a high loading of fine particles and high fractions of secondary species of sulfates, nitrates and ammonium (SNA) in the fine particles (Sun *et al.*, 2006; Wang *et al.*, 2012; Liu *et al.*, 2013). Thus, understanding the formation mechanism of SNA will help understand the formation mechanism of haze. Secondary sulfate was produced under tropospheric conditions via both gas- and aqueous-phase processes (Seinfeld and Pandis, 2006). With respect to gas-phase processes, SO_2 oxidation by the OH radical followed by gas-to-particle conversion dominates (Stockwell and Calvert, 1983). Sulfate formation in aqueous solution is generated by the uptake of SO_2 onto wet, pre-existing particles or cloud droplets followed by oxidation by O_3, H_2O_2, NO_2 or O_2 catalyzed by Fe(III) and Mn(II) (Seinfeld and Pandis, 2006; Wang *et al.*, 2012). Previous studies found that sulfate is produced mainly by heterogeneous reactions by oxidizing SO_2 on wet, pre-existing particles or cloud droplets under high relative humidity (RH) conditions in haze episode in winter (Sun *et al.*, 2006; Li *et al.*, 2011; Wang *et al.*, 2012; Zhao *et al.*, 2013). Both laboratory experiments and in situ observations suggest that the aqueous oxidation of SO_2 is attributed to catalysis by metals, such as iron and manganese (Turšič *et al.*, 2003; Li *et al.*, 2011; Wang *et al.*, 2012). The formation pathway of nitrates, however, is less well known compared to the formation of sulfate, and it is influenced by the emission load of the precursors, the concentrations of oxidants in both the gas and the liquid phase, the characteristics of pre-existing particles and meteorological conditions (Seinfeld and Pandis, 2006; Pathak *et al.*, 2009; Guo *et al.*, 2010; Ye *et al.*, 2011; He *et al.*, 2012). Generally, fine nitrate is more concentrated in homogeneous gas-phase reactions between ammonia and nitric acid in ammonium-rich conditions and is attributed to heterogeneous hydrolysis of N_2O_5 on the surface of humid and acidic pre-existing particles under ammonium-poor conditions (Seinfeld and Pandis, 2006; Pathak *et al.*, 2009). He *et al.* (2013) suggests aerosol acidity instead of ammonium rich/poor conditions as the key parameter to investigate the formation pathways of nitrate.

However, most previous studies focused on filter measurements with low time resolution or sampling artifacts such as evaporative loss, whereas the haze pollution varies fast in the atmosphere due to the influences of air-pollutant emission, secondary processes and so on. Hence, measurement with high time resolution and fewer sampling artifacts is crucial to characterize the real-time change of the chemical, physical, and optical properties of haze and to understand the formation mechanism of haze. Sun *et al.* (2014) studied the source and evolution mechanisms of the heavy haze episode that occurred in January, 2013 in Beijing with the high time resolution of the Aerodyne Aerosol Chemical Speciation Monitor (ACSM), and found that the formation and evolution of haze pollution was mainly produced by four factors: stagnant meteorological conditions, coal burning, secondary processes and regional transport.

In previous study, we generally discussed the formation and evolution mechanism of a regional haze episode in megacity Beijing from 20 September to 27 September, 2011 (Liu *et al.*, 2013). Particle mass concentration and size distribution, aerosol optical properties, gas pollutants and meteorological parameters were measured. We found that the formation and evolution of this haze episode was mainly affected by stable anti-cyclone synoptic conditions at the surface, PBL (planetary boundary layer) height decreasing, heavy emissions of pollutants and hygroscopic growth of aerosol. In this study, we focus on investigating the secondary formation mechanism of sulfate and nitrate in detail to explore the secondary processes of the haze episode by real-time and high time resolution instruments.

METHODS

Experimental Site

Beijing is located on the northern edge of the North China Plain, surrounded by high mountains in the west, north, and northeast, which is disadvantageous for air-pollutant dispersion (Fig. 1). The meteorological observation were made at Peking University on the roof of the Atmospheric and Oceanic Sciences Department, Physics School (39.98°N, 116.35°E), and the monitoring instruments for atmospheric pollutants were located on the roof of the Environmental Science and Engineering College, Peking University, which is 200 meters away from the meteorological observation instrument. The ACSM and LIDAR were performed on the roof of a building (~8 m above ground level) at the Institute of Atmospheric Physics (IAP), Chinese Academy of Sciences (39.91°N, 116.37°E). The observation site is approximately 0.9 km to the north of 3rd ring road. Inversion of the boundary-layer height was based on observational data from the LIDAR.

Instrumentation and Measurements

All of the observation instruments involved in this study except ACSM were described in detail in Liu *et al.* (2013), and the time series of the meteorological parameters are illustrated in Fig. 2. The submicron aerosol was measured in situ from 20 September to 27 September, 2011 by ACSM. The Aerodyne Aerosol Chemical Speciation Monitor (ACSM) is specially designed recently for long-term continuous measurements of the mass concentration and chemical components (OM (organic materials), Cl^-, NO_3^-, SO_4^{2-} and NH_4^+) of $PM_{1.0}$ (particulate matter with an aerodynamic diameter equal or less than 1 μm) at a time resolution of ~15 min. The detailed descriptions and evaluation of ACSM have been given in Ng *et al.* (2011) and Sun *et al.* (2012). The temporal resolution of each instrument varied, and the data were averaged to 1h during data processing and analysis.

Two day air-mass back trajectories arriving at the sampling site during the measurement period were calculated by the HYSPLIT-4 (Hybrid Single-Particle Lagrangian Integrated Trajectory) model (U.S. National Oceanic and Air Administration/Air Resources Laboratory) with a 1° × 1° latitude–longitude grid and final meteorological database.

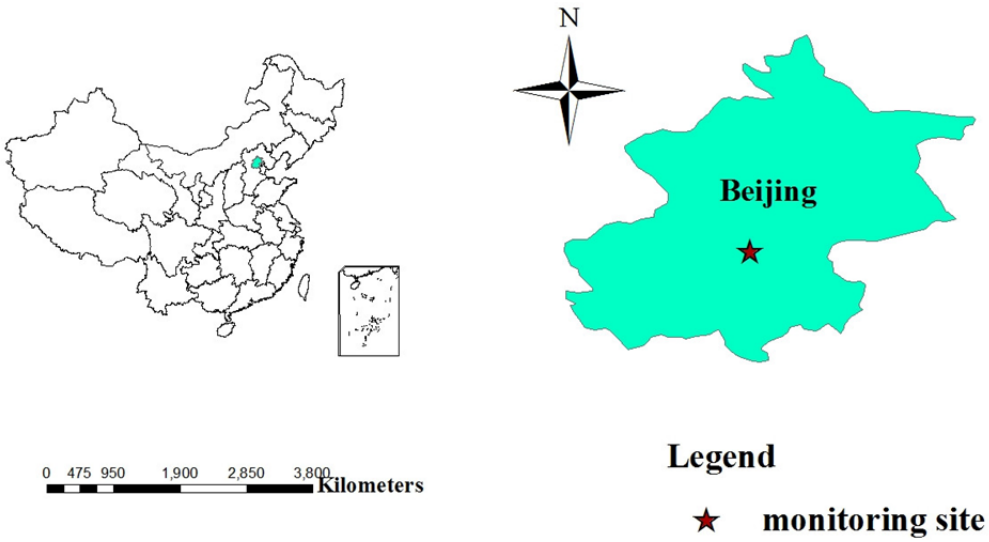

Fig. 1. Schematic diagram of the monitoring site.

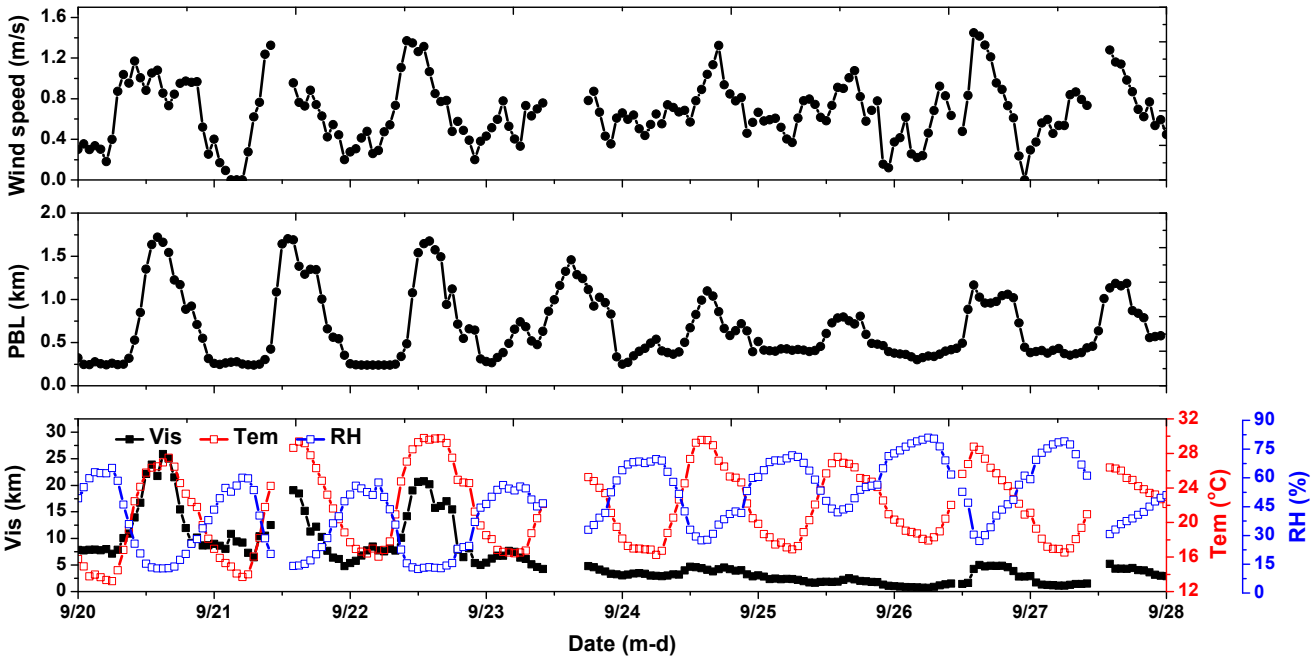

Fig. 2. Time series of meteorological parameters (wind speed, PBL, visibility, temperature and RH) in Beijing from 20–27 September 2011.

The six hourly final archive datasets were obtained from the GDAS (National Center for Environmental Prediction's Global Data Assimilation System) wind field reanalysis. The HYSPLIT-4 model is described in detail on the website (http://www.arl.noaa.gov/ready/open/hysplit4.html). The backward air trajectories are presented in Fig. 3.

RESULTS AND DISCUSSION

Meteorological Condition and Pollutant Concentrations

Meteorological Conditions

Fig. 2 shows the meteorological parameters in Beijing from 20–27 September 2011. The visibility was below 10 km (the mean value is 3.6 km), and RH was less than 90% with no precipitation, which indicated that a haze episode occurred from 23 to 27 September. Thus, a non-haze episode was defined from 20–22 September. During the haze episode, the wind speed was relatively low with a mean value of 0.7 m s^{-1}, and there were no strong pressure gradients over Beijing (as discussed in Liu *et al.* (2013)), which meant relatively weak air circulation over the region. This relatively stable synoptic condition limited the dispersion of air pollutants and led to an increase in the pollutant concentrations. As discussed in Liu *et al.* (2013), a slowly migrating high pressure system overlaid Beijing and the air mass was sinking in the vertical direction during the

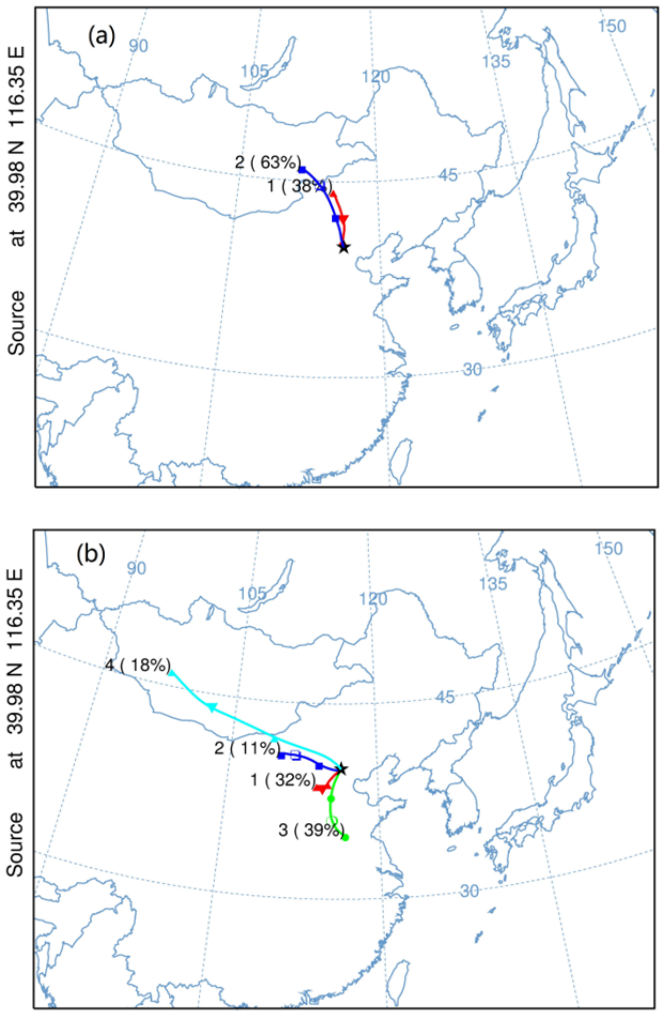

Fig. 3. Two-day backward air trajectories arriving at PKU, Beijing on 20–22 September (a) and 23–27 September (b). Data in brackets denotes the fraction of the air mass.

formation of haze, which caused the further accumulation of pollutants. In addition, the daily maxima PBL height decreased from 1.7 km on 20–22 September to 0.75 km on 25 September. A low height of PBL would retain the pollutants in the ground layer and favor the formation of regional haze (decreasing the height of PBL is discussed in detail by Liu *et al.* (2013)). Meanwhile, RH was relatively high with a mean value of 55.5%, compared with RH in non-haze episode (a mean value of 34.4%), which favored hygroscopic growth of ambient particles and heterogeneous reactions of gaseous precursors (Liu *et al.*, 2010; Wang *et al.*, 2012; Zhao *et al.*, 2013).

In a non-haze episode, all of the trajectory clusters were from the north or northwest of Beijing, originating from Mongolia and then passing through the northeast region of Inner Mongolia. These areas are mainly desert and the semi-desert regions with less anthropogenic pollutions. However, the trajectory clusters mainly originated from the south and southwest provinces of Beijing (accounting for approximately 71%) in a haze episode and traveled over Shandong and Hebei, where highly polluted cities, such as Tianjin and Tangshan, are located. The levels of secondary species (SO_4^{2-}, NO_3^-, and NH_4^+), OM and EC were observed to be much higher in the air mass from the south and southwest than in the air mass from the north or northwest of Beijing (Sun *et al.*, 2006; Zhang *et al.*, 2013). Higher concentrations of secondary species and OM were also found in this study (Fig. 6). Thus, air parcels transported through the south and southwest of Beijing bring more air pollutants to Beijing and favor the formation of haze.

Temporal Variations of Atmospheric Pollutants

Fig. 4 shows the temporal variations of the measured PM_{10}, $PM_{2.5}$, ratio of $PM_{2.5}/PM_{10}$, NO, NO_2, SO_2, O_3 and CO in Beijing from 20–27 September 2011. There was a significant upward trend of $PM_{2.5}$, PM_{10} and $PM_{2.5}/PM_{10}$: the average $PM_{2.5}$ and PM_{10} concentrations and $PM_{2.5}/PM_{10}$ ratio increased from 37.6 μg m^{-3}, 91.7 μg m^{-3} and 0.42, respectively, in a non-haze episode to 116.8 μg m^{-3}, 190.9 μg m^{-3} and 0.60, respectively, in a haze episode. Higher particle pollutants, especially fine particles, on a haze day were also found by other studies (Sun *et al.*, 2006; Liu *et al.*, 2013; Zhao *et al.*, 2013; Sun *et al.*, 2014), which indicated that the haze was caused by fine particles.

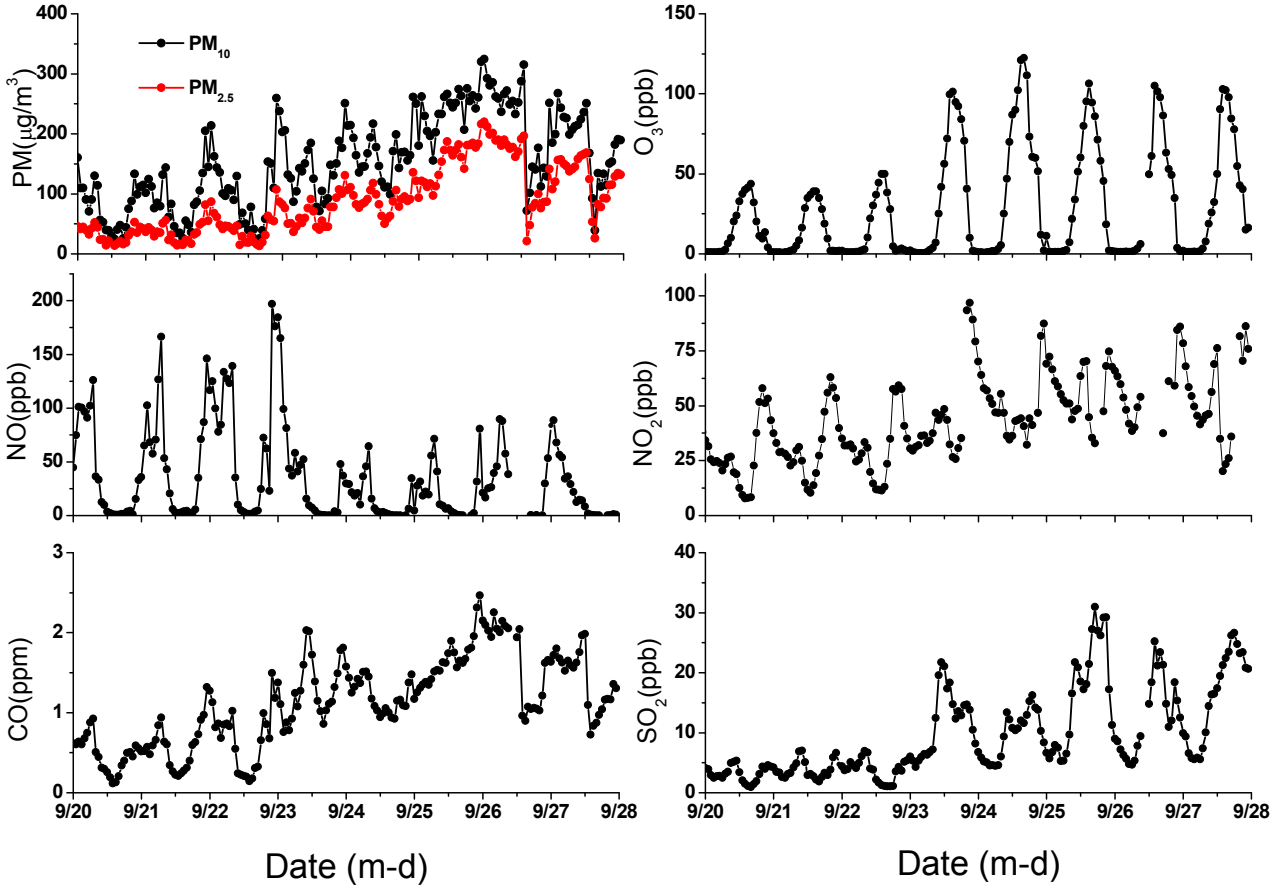

Fig. 4. Time series of PM_{10}, $PM_{2.5}$ and gaseous pollutants.

Generally, the averaged concentrations of the air pollutants CO, CO_2, SO_2, NO_2 and O_3 significantly increased: from 0.58 ppm, 410.49 ppm, 3.59 ppb, 30.26 ppb and 14.07 ppb, respectively, in non-haze episodes to 1.44 ppm, 430.11 ppm, 13.23 ppb, 52.15 ppb and 36.56 ppb, respectively, in haze episodes, which was in accordance with other studies (Zhao *et al.*, 2013). The averaged NO concentration fell by nearly half from 51.69 ppb in non-haze episodes to 26.63 ppb in haze episodes, which was probably oxidated by photochemistry process. The sharp increase of the gas precursors during the haze episode was ascribed to the following factors. First, the low height of PBL would retain the gas precursors in the surface layer, and the stable synoptic condition limited the vertical and horizontal diffusion of pollutants, which led to an increase of gas precursors and the formation of haze. Second, pollutants are regionally transported from heavily polluted areas in the south and southwest provinces of Beijing. CO, SO_2, NO_2, NO and CO_2 resulted mainly from primary emissions, including the emissions of coal combustion and vehicle exhaust. The two-day backward air trajectories arriving at PKU in haze episodes (Fig. 3) were shown mainly from the south and southwest provinces of Beijing, where heavy industry and coal combustion were located. The spatial distribution of the annual mean fine aerosol optical depth (AOD) retrieved from the MODIS satellite remote sensing is discussed in Liu *et al.* (2013). Obvious pollution existed in the south and southwest provinces of Beijing before and during the haze episodes, which indicated that the air mass passing through these areas would bring pollutants into Beijing and favor the formation of haze. Thus, regional transport from the polluted south and southwest provinces of Beijing significantly attributed to a sharp increase of the pollutants during the haze episodes.

Time series of OM, SO_4^{2-}, NO_3^-, NH_4^+ and Cl^- in $PM_{1.0}$ measured by ACSM were presented in Fig. 5. All of the measured chemical species showed a significant upward trend from non-haze episodes to haze episodes, especially for the secondary pollutants SO_4^{2-}, NO_3^- and NH_4^+ (SNA): the averaged concentrations increased from 21.3, 0.8, 1.8, 1.0 and 0.2 μg m^{-3}, respectively, for OM, SO_4^{2-}, NO_3^-, NH_4^+ and Cl^- in non-haze episodes to 49.9, 20.6, 29.6, 18.7 and 2.3 μg m^{-3} in haze episodes. The growth rate of SNA far exceeded that of OM (approximately ten times higher) when haze formed, which indicated that secondary processes of SNA significantly strengthened when haze formed (discussed in section 3.2). Additionally, the proportions of OM, SO_4^{2-}, NO_3^-, NH_4^+ and Cl^- in $PM_{1.0}$ measured by ACSM illustrated sharp differences for non-haze episodes and haze episodes (Fig. 6). The fractions of SNA were higher in a haze episode (~57%) than in a non-haze episode (~14%), whereas the OM fraction was just the opposite, which was in accordance with previous studies (Sun *et al.*, 2006; Wang *et al.*, 2012; Zhao *et al.*, 2013).

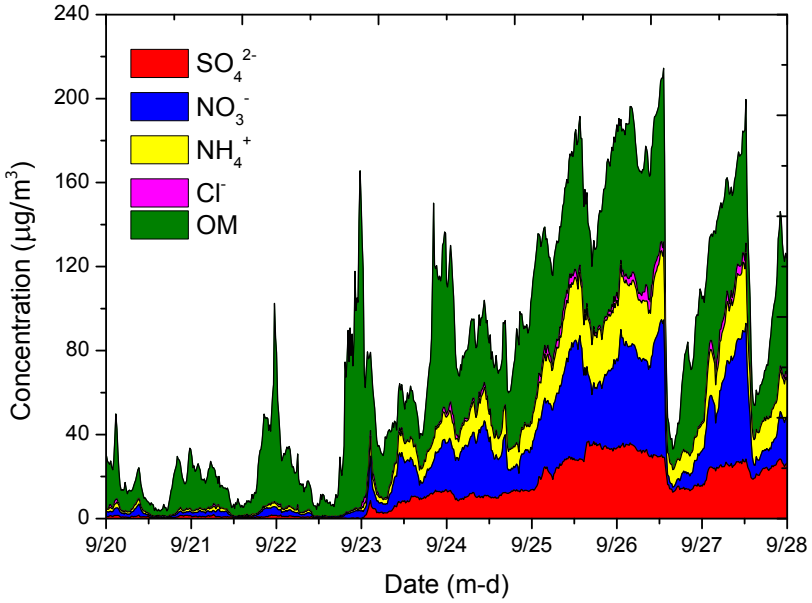

Fig. 5. Time series of OM, SO_4^{2-}, NO_3^-, NH_4^+ and Cl^- in $PM_{1.0}$ measured by ACSM.

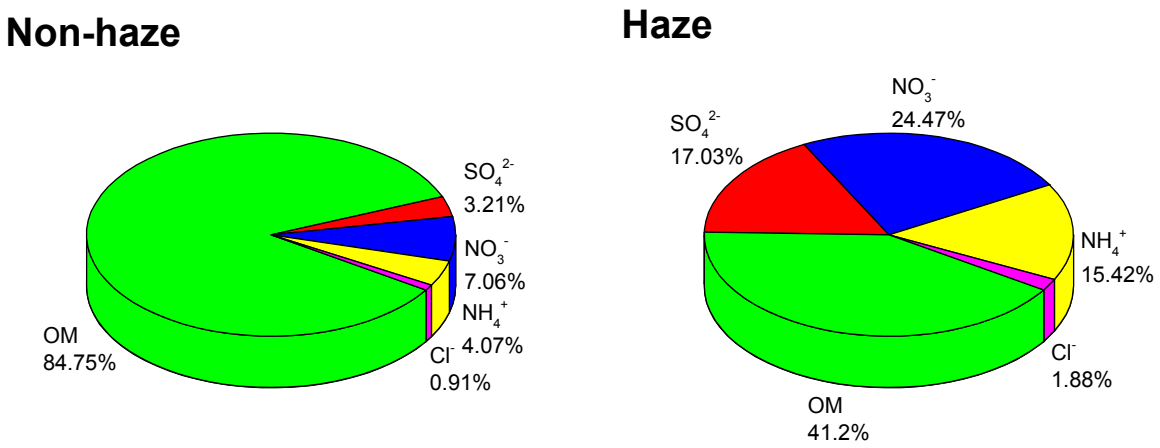

Fig. 6. Proportions of OM, SO_4^{2-}, NO_3^-, NH_4^+ and Cl^- measured by ACSM in non-haze and haze episodes.

Secondary Formation of Sulfate in Haze Episodes

As illustrated in Fig. 5, the sulfate concentration continuously increased during the multi-day haze episodes by secondary processes. The sulfur oxidation ratio SOR = $nSO_4^{2-}/(nSO_4^{2-} + nSO_2)$ (n refers to the molar concentration) is used in this study (Sun *et al.*, 2006; Wang *et al.*, 2006; Zhao *et al.*, 2013) to estimate the degree of secondary formation of sulfate.

As shown in Fig. 7, the SOR ratio presented an upward trend from a non-haze episode to a haze episode: the average value of SOR was 0.05 in non-haze episodes with a highest value of 0.11, whereas the average value of SOR was 0.27 in haze episodes with a highest value of 0.62, which indicated more intense secondary formation of sulfate in haze episodes. Previous studies suggested that the conversion of SO_2 to sulfate during a haze episode in winter was mainly through the aqueous-phase oxidation of SO_2 by the catalytic oxidation of iron and manganese with weak photochemical activity (low O_3 concentration, high NO_2 concentration and low temperature) during the haze period (Sun *et al.*, 2006; Li *et al.*, 2011; Wang *et al.*, 2012; Zhao *et al.*, 2013). To evaluate the effect of gas-phase oxidation of SO_2 during the haze period, we analyzed the correlations of SOR with O_3 and temperature in haze episodes and found that low correlations existed between SOR and O_3 ($r = -0.53$, $p = 0.01$) and SOR and temperature ($r = -0.53$, $p = 0.01$). In addition, SOR showed evident diurnal variation with a high value before dawn when the concentration of O_3 was low and the concentration of NO_2 was high, and a low value in the afternoon when the concentration of O_3 was high and the concentration of NO_2 was low in a haze episode, which indicated that the photochemical activity had an insufficient effect on the gas-phase conversion of SO_2 to sulfate in haze episodes. However, SOR and RH exhibited a high correlation ($r = 0.84$, $p = 0.01$) in haze episodes and a poor correlation in non-haze episodes ($r = 0.22$, $p = 0.21$), which was in accordance with other studies (Sun *et al.*, 2006; Sun *et al.*, 2013). To investigate the effects of RH on SOR during a

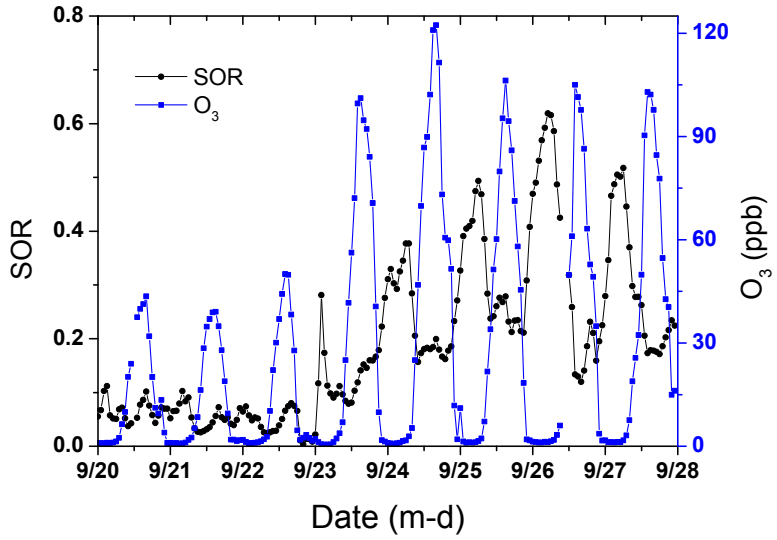

Fig. 7. Time series of SOR and O_3 during the monitoring period.

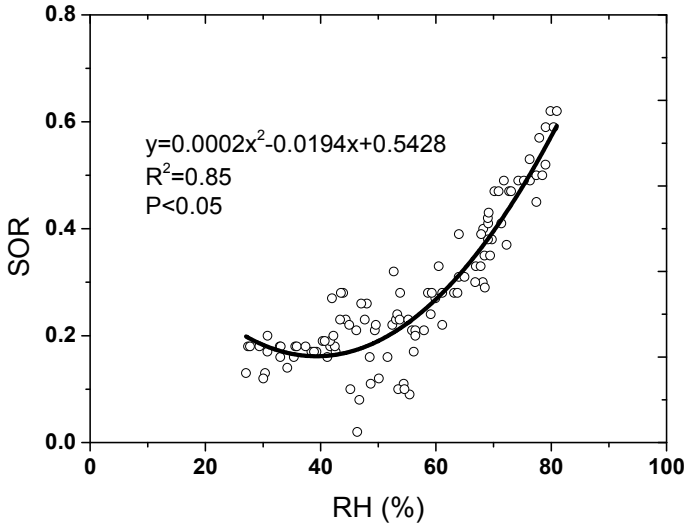

Fig. 8. Scatter plot of SOR versus RH in haze episodes of 23–27 September, 2011.

haze period, a scatter plot was shown of SOR versus RH in haze episodes (Fig. 8), and curve fitting was performed to explore the relationship between SOR and RH. The relationship between the SOR ratio and RH could be fitted by the function ($y = 0.0002x^2 – 0.0194x + 0.5428$, $R^2 = 0.85$). As illustrated in Fig. 8, the SOR ratio was enhanced with rising RH. If the average RH was below 45%, the SOR ratio was generally lower than 0.2. Once the RH was above 45%, the ratio of SOR increased sharply, with a maximum of 0.62 at the RH of 80%. This might be attributed to higher liquid water content in the aerosols at high RH, which enhanced the heterogeneous formation of sulfate (Wang *et al.*, 2012). Thus, sulfate was mainly produced by the aqueous-phase oxidation of SO_2 rather than the gas-phase conversion of SO_2 to sulfate in haze episodes in Beijing, which was similar to the results of previous studies (Sun *et al.*, 2006, 2013; Zhao *et al.*, 2013). However, the O_3 concentration was high in our study compared with previous studies observed in winter when the O_3 concentration was low (5 ppb, Zhao *et al.*, 2013; 5.4 ppb, Wang *et al.*, 2012), which indicated that sulfate was produced mainly by heterogeneous processes instead of gas-phase processes in haze episodes for both high and low photochemical activity atmospheres.

Furthermore, because the heterogeneous processes of sulfate occurred on the wet surfaces of particles, we analyzed the relationship between SOR and the surface area (dS) of particles smaller than 1 μm (Fig. 12) to confirm the heterogeneous processes of sulfate in haze episodes. As presented in Fig. 12, the SOR ratio grew linearly with the particle surface area and significantly correlated with particle surface area (dS) with the regression function ($y = 2.78E – 4x + 0.03$, $R^2 = 0.71$). In addition, dS increased with RH rising, with high correlation of $r = 0.64$, which might be due to hygroscopic growth of ambient particles. Thus, particle surface area significantly contributed to the enhanced sulfate formation on haze day, which might be due to more SO_2

gas and oxidants (O_3, H_2O_2 or O_2) dissolved onto the humid particle surface and enhanced the heterogeneous production of sulfate and improved the SOR ratio on the haze day.

Secondary Formation of Nitrate in Haze Episodes

With the growth of NOx emissions in recent years, the concentration and proportion of nitrate in particles are found to have increased significantly in most Chinese megacities (Zhang *et al.*, 2007; Chan and Yao, 2008; Shen *et al.*, 2008). As shown in Fig. 5, an obvious increase of nitrates was also observed during haze episodes, and nitrates dominated SNA during the measurement periods (discussed in section 3.1.2), which implied that nitrate had become a major concern during haze pollution.

Fig. 9 shows the correlation of measured NH_4^+ with predicted NH_4^+ that is required to fully neutralize Cl^-, NO_3^- and SO_4^{2-} (predicted NH_4^+ (= 18 × (2 × SO_4^{2-}/96 + NO_3^-/62 + Chl/35.5)). A slope of higher than 1 (slope = 1.04) indicates that almost complete neutralization of Cl^-, NO_3^- and SO_4^{2-} during the monitoring period; therefore, the samples are in ammonium-rich conditions. Cl^-, NO_3^- and SO_4^{2-} are components of $PM_{1.0}$ measured by ACSM. Figs. 10(a) and 10(b) present scatter plots of the nitrate-to-sulfate molar ratio ($[NO_3^-]/[SO_4^{2-}]$) versus the ammonium-to-sulfate molar ratio ($[NH_4^+]/[SO_4^{2-}]$) during haze and non-haze periods, which is used as an indication of the pathway of NO_3^- formation (Pathak *et al.*, 2009). As shown in Figs. 10(a) and 10(b), the molar ratio of $[NO_3^-]/[SO_4^{2-}]$ grew linearly with the $[NH_4^+]/[SO_4^{2-}]$ molar ratio in NH_4^+-rich conditions in both haze and non-haze episodes with significant correlations (r = 0.75, p = 0.01 and 0.95, p = 0.01, respectively in non-haze and haze episodes), which indicated that the formation of aerosol NO_3^- was dominated by the homogenous reaction of $HNO_3(g) + NH_3(g) \leftrightarrow NH_4NO_3(s, aq)$ (Pathak *et al.*, 2009; He *et al.*, 2012). To demonstrate the homogenous formation of nitrate, a scatter plot of the molar concentrations of nitrate and "excess ammonium" is shown in Figs. 10(c) and 10(d), and "excess ammonium" is defined as $[NH_4^+]_{Excess}$ = ($[NH_4^+]/[SO_4^{2-}] - 2.29$) × $[SO_4^{2-}]$ for non-haze episodes, and $[NH_4^+]_{Excess}$ = ($[NH_4^+]/[SO_4^{2-}] - 2.58$) × $[SO_4^{2-}]$ for haze episodes (the constants of 2.29 and 2.58 were the intercept of the regression line of $[NO_3^-]/[SO_4^{2-}]$ versus $[NH_4^+]/[SO_4^{2-}]$ with the axis, respectively on non-haze and haze day (He *et al.*, 2012)). As illustrated in Figs. 10(c) and 10(d), the nitrate molar concentrations increased with the excess ammonium molar concentrations for both haze and non-haze episodes: the regression functions were y = 0.59x + 5.19 (R^2 = 0.57) and y = x + 21.81 (R^2 = 0.98), respectively in non-haze and haze episodes, which suggested that nitrate was mainly produced by the homogenous reaction mentioned above after ammonium neutralized most of the sulfate. A shallower slope (0.59) was found in non-haze day, which indicated that in $PM_{1.0}$ there was approximately 41% excess NH_4^+ bounded to other species like Cl^- (NH_4Cl).

Because the nitrate concentration obviously increased during the haze episodes, the nitrogen oxidation ratio NOR = $nNO_3^-/(nNO_3^- + nNO_2)$ (n refers to the molar concentration) is used in this study to estimate the degree of secondary formation of nitrate (Sun *et al.*, 2006; Wang *et al.*, 2006; Zhao *et al.*, 2013). The NOR ratio with an average ratio of 0.12 and a highest ratio of 0.26 in haze episodes was significantly higher than the NOR ratio with an average ratio of 0.01 and a highest ratio of 0.03, which indicated that nitrate formation was significantly enhanced in haze episodes. Additionally, the molar ratios of both ($[NO_3^-]/[SO_4^{2-}]$) and ($[NH_4^+]/[SO_4^{2-}]$), and molar concentrations of nitrate and "excess ammonium", presented better correlation in haze episodes than in non-haze episodes, which suggested that the homogenous production of nitrate was strongly enhanced in haze episodes.

The thermodynamic equilibrium reaction of $HNO_3(g) + NH_3(g) \leftrightarrow NH_4NO_3(s, aq)$ was influenced by the ambient temperature, RH and the characteristics of the pre-existing particles (Pakkanen *et al.*, 1996; Seinfeld and Pandis, 2006;

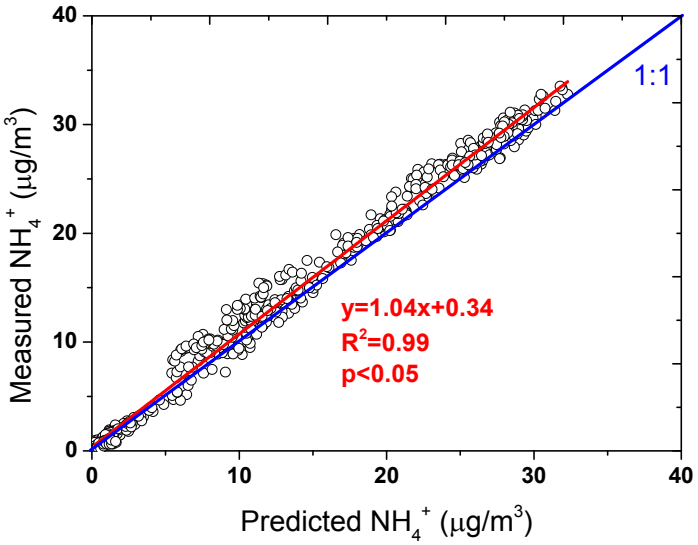

Fig. 9. Correlation between measured NH_4^+ and predicted NH_4^+ (= 18 × (2 × SO_4^{2-}/96 + NO_3^-/62 + Chl/35.5) during the monitoring period.; Cl^-, NO_3^- and SO_4^{2-} are components of $PM_{1.0}$ measured by ACSM.

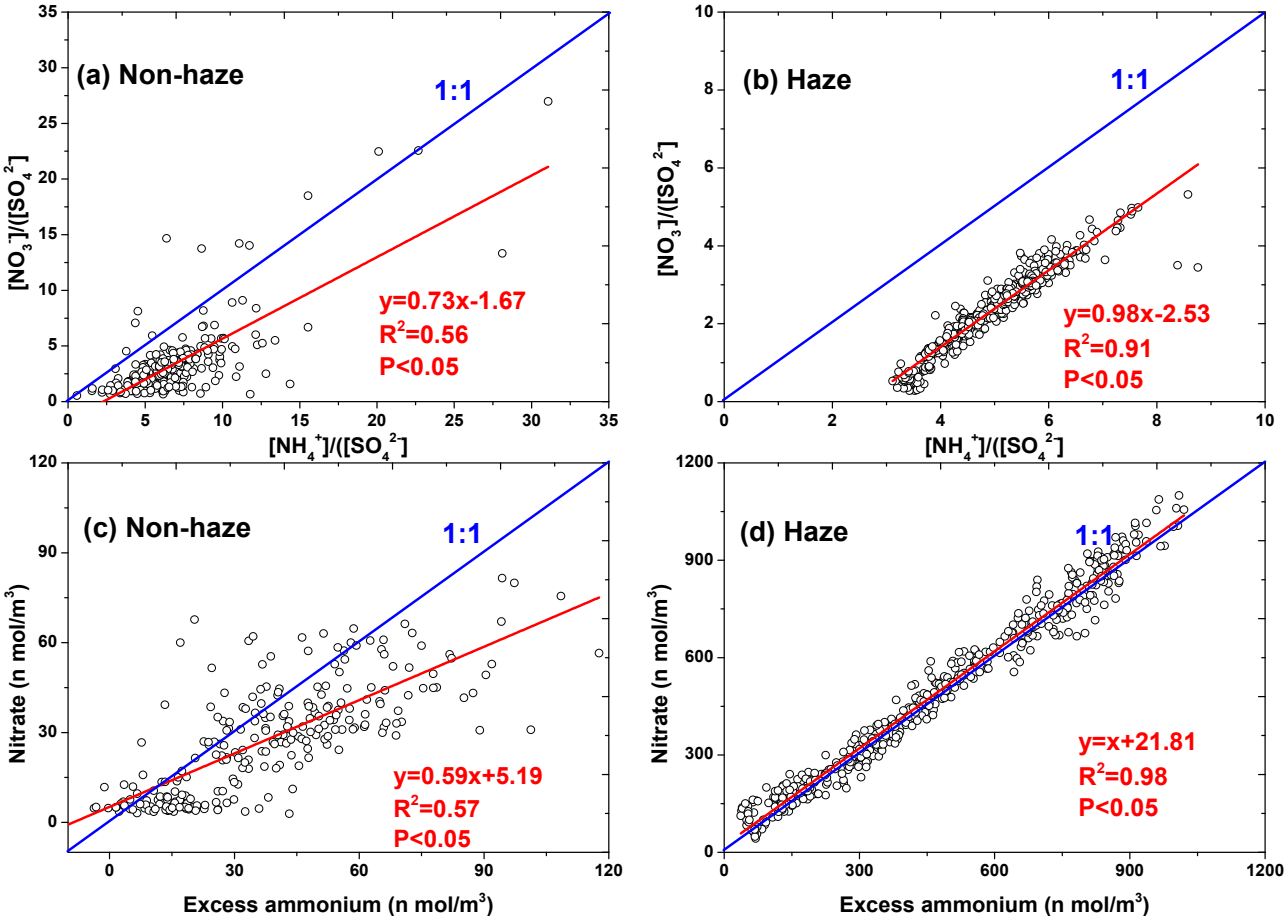

Fig. 10. Molar ratios of $[NO_3^-]/[SO_4^{2-}]$ versus $[NH_4^+]/[SO_4^{2-}]$ in (a) non-haze of 20–22 September and (b) haze episodes of 23–27 September; scatter plot of the molar concentrations of $[NO_3^-]$ versus the molar concentrations of $[NH_4^+]_{Excess}$ in (c) non-haze and (d) haze episodes.

Ianniello *et al.*, 2011; Wang *et al.*, 2012). The thermodynamic equilibrium constant Ke for solid NH_4NO_3 was calculated as a function of temperature: lnKe = 84.6 – 24220/T – 6.1ln(T/298) (Stelson and Seinfield, 1982). However, for deliquescent particles, Ke was considerably reduced by the coexistence of sulfated, so the NH_4NO_3 ion strength fraction Y = $[NH_4NO_3]/([NH_4NO_3] + 3[(NH_4)_2SO_4])$ was brought in and calculated according to Stelson and Seinfield (1982). Then the new equilibrium dissociation constant Ke' was derived by multiplying Ke with Y. Fig. 11 shows the scatter plot of equilibrium constant Ke', RH and the temperature in haze and non-haze episodes. As illustrated in Fig. 11, the theoretical equilibrium constant Ke' followed the function of temperature in both haze and non-haze episodes, which was in accordance with previous studies (Guo *et al.*, 2010; Ianniello *et al.*, 2011); while nearly a quarter of points in haze episode did not follow the function with sharply smaller Ke'. These points were mainly distributed in RH higher than 66%, where deliquescent particles existed and the NH_4NO_3 ion strength fraction Y was used in Ke' calculation. In addition, these points were mainly distributed at about 1:00–7:00 am, so we compared the data at 1:00–7:00 am in haze and non-haze episodes (Fig. 13). The mean value of Ke' in haze day (Ke' = 2.32) was slightly lower than in non-haze day (Ke' = 2.38), and the mean value of NOR in haze episode (0.129) was sharply higher than in non-haze episode (0.006), which suggested that the high RH in haze episode might significantly enhance the homogeneous production of nitrate. Moreover, Ke' grew linearly with SO_4^{2-} concentration increasing with regression function of $y = 0.04x + 1.22$ ($R^2 = 0.21$) during 1:00–7:00 am in haze episode, which indicated that the sulfate content in particles impacted on the thermodynamic equilibrium constant of Ke'. Therefore, higher RH in haze episodes reduced the thermodynamic equilibrium constant Ke', and favored the thermodynamic equilibrium reaction of $HNO_3(g) + NH_3(g) \leftrightarrow NH_4NO_3(s, aq)$ to formed nitrate, which might help explain the enhanced the homogenous production of nitrate in haze episodes.

Furthermore, we analyzed the relationship between NOR and the surface area (dS) of particles smaller than 1 μm (Fig. 12) to explore the influence of the particle surface area on the production of nitrate. As illustrated in Fig. 12, the NOR ratio was enhanced as the particle surface area rose and significantly correlated with the particle surface area (dS) with an exponential fit function of $y = 0.0083e^{0.0025x}$ ($R^2 = 0.70$). If the average particle surface area was lower than 700 $\mu m^2\ cm^{-3}$, the NOR ratio was generally below 0.05.

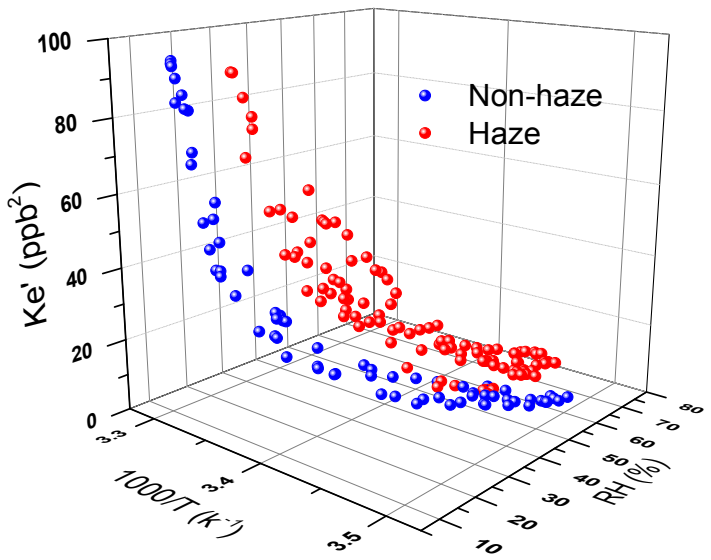

Fig. 11. Scatter plot of equilibrium constant Ke', RH and the temperature in haze and non-haze episodes.

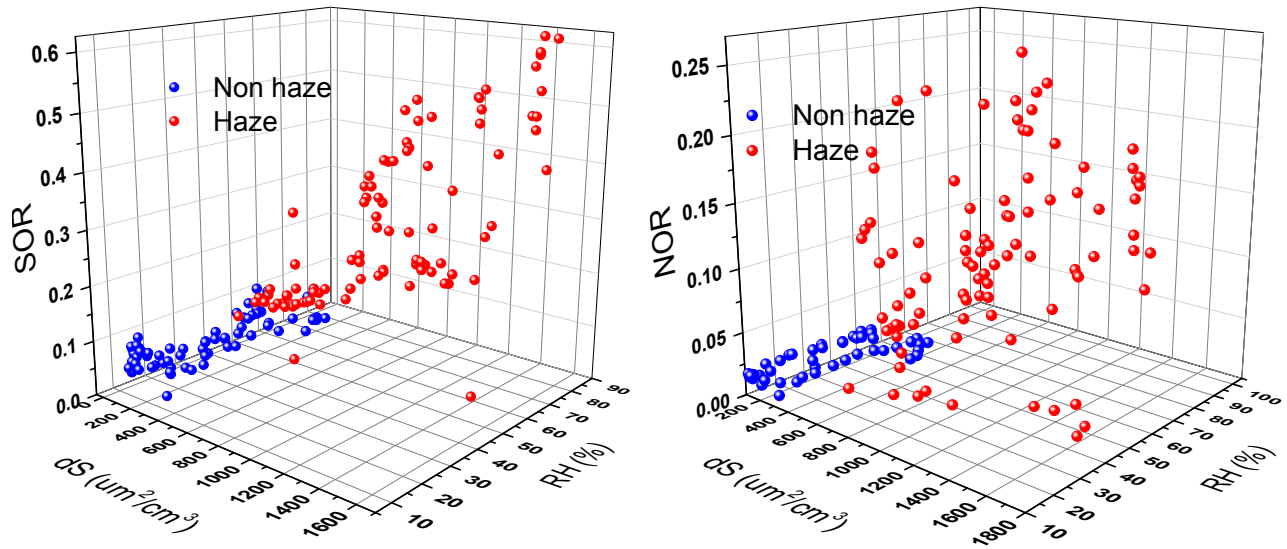

Fig. 12. Scatter plot of SOR, dS and RH; NOR, dS and RH during haze and non-haze episodes.

However, if the average particle surface area was higher than 700 μm^2 cm^{-3}, the NOR ratio increased sharply with a maximum of 0.26 at a particle surface area of 1140 μm^2 cm^{-3}. Compared to the sulfates, the variation of NOR was less consistent with RH rising, and showed no significant correlation with RH (r = 0.05 in haze episodes), which indicated heterogeneous reactions did not significantly contributed to the enhanced nitrate formation in haze episodes. Therefore, the particle surface area significantly contributed to the enhanced homogeneous production of nitrate in haze episodes.

CONCLUSIONS

Meteorological and air-pollutant measurements were used during a heavy haze episode in Beijing from 20 September to 27 September, 2011 to explore the secondary processes in the haze episode. The relatively stable synoptic conditions and regional transport from polluted areas in the south and southwest of Beijing favored the haze formation. $PM_{2.5}$, PM_{10} and $PM_{2.5}/PM_{10}$ significantly increased during the haze period (with average $PM_{2.5}$ and PM_{10} concentrations and a $PM_{2.5}/PM_{10}$ ratio of 116.8 μg m^{-3}, 190.9 μg m^{-3} and 0.60, respectively), which indicated that the haze was caused by fine particles. In addition, the concentrations of secondary inorganic pollutants (SO_4^{2-}, NO_3^- and NH_4^+) were found sharply increased in haze episode, which indicated that secondary processes significantly strengthened in haze episode. Intense secondary formation of sulfate was observed in haze episode, which was mainly produced by the aqueous-phase oxidation of SO_2 rather than the gas-phase conversion of SO_2 to sulfate in haze episode in Beijing. Furthermore, the relationship between SOR and the surface area (dS) of particles smaller than 1 μm was analyzed, and and SOR

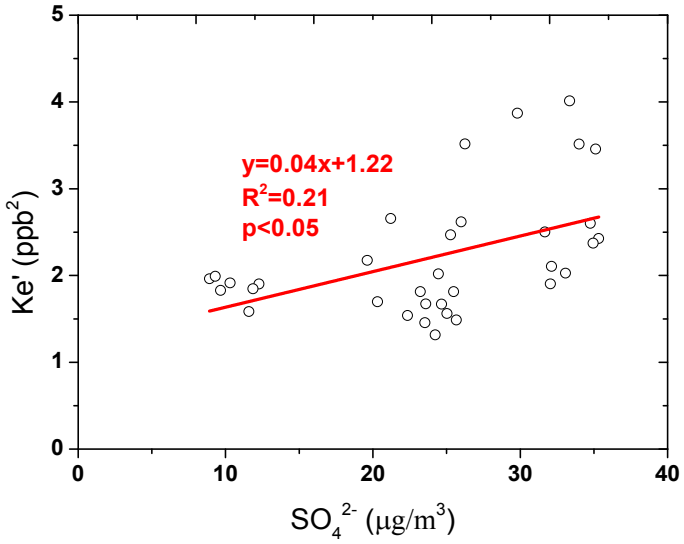

Fig. 13. Scatter plot of Ke' and SO_4^{2-} during 1:00 – 7:00 am in haze episode.

grew linearly with dS (R^2 = 0.71). In addition, dS increased with RH rising, with high correlation of r = 0.64, which might be due to hygroscopic growth of ambient particles. Thus, particle surface area significantly contributed to the enhanced sulfate formation in haze episode, which might be due to more SO_2 gas and oxidants (O_3, H_2O_2 or O_2) dissolved onto the humid particle surface and enhanced the heterogeneous production of sulfate and improved the SOR ratio during the haze periods. Intense secondary formation of nitrate was also found in haze episode, which was mainly due to the homogenous reaction under ammonium-rich conditions mentioned in this study. The thermodynamic equilibrium constant Ke' was calculated in our study, and we analyzed the effects of temperature, RH, and sulfate content in the particles on it. Higher RH in haze episode reduced the thermodynamic equilibrium constant Ke', and favored the thermodynamic equilibrium reaction of $HNO_3(g) + NH_3(g) \leftrightarrow NH_4NO_3(s, aq)$ to formed nitrate, which might help explain the enhanced homogenous production of nitrate in haze episode. Additionally, a good empirical fit (R^2 = 0.70) between NOR and dS were found in this study, while the variation of NOR was less consistent with RH rising (r = 0.05 in haze episodes), which indicated that the particle surface area significantly contributed to the intense homogeneous production of nitrate in haze episodes.

ACKNOWLEDGEMENT

This work was supported by the National Natural Science Foundation of China (Grant No. 41475113 and No. 41175018), and by the CAS Strategic Priority Research Program (Grant No. XDB05010500).

REFERENCE

Chan, K.C. and Yao, X. (2008). Air Pollution in Mega Cities in China. *Atmos. Environ.* 42: 1–42.

Guo, S., Hu, M., Wang, Z.B., Slanina, J. and Zhao, Y.L. (2010). Size-resolved Aerosol Water-soluble Ionic Compositions in the Summer of Beijing: Implication of Regional Secondary Formation. *Atmos. Chem. Phys.* 10: 947–959.

He, K., Zhao, Q., Ma, Y., Duan, F., Yang, F., Shi, Z. and Chen, G. (2012). Spatial and Seasonal Variability of $PM_{2.5}$ Acidity at Two Chinese Megacities: Insights into the Formation of Secondary Inorganic Aerosols. *Atmos. Chem. Phys.* 12: 1377–1395.

Ianniello, A., Spataro, F., Esposito, G., Allegrini, I., Hu, M. and Zhu, T. (2011). Chemical Characteristics of Inorganic Ammonium Salts in $PM_{2.5}$ in the Atmosphere of Beijing (China). *Atmos. Chem. Phys.* 11: 10803–10822.

Li, W.J., Zhou, S., Wang, X., Xu, Z., Yuan, C., Yu, Y., Zhang, Q. and Wang, W. (2011). Integrated Evaluation of Aerosols from Regional Brown Hazes over northern China in Winter: Concentrations, Sources, Transformation, and Mixing States. *J. Geophys. Res.* 116: D09301, doi: 10.1029/2010JD015099.

Liu, X.G., Li, J., Qu, Y., Han, T.T., Hou, L., Gu, J.W., Chen, C., Yang, Y.R., Liu, X.Y., Yang, T., Zhang, Y.H., Tian, H.Z. and Hu, M. (2013). Formation and Evolution Mechanism of Regional Haze: A Case Study in Mega-city Beijing of China. *Atmos. Chem. Phys.* 13: 4501–4514.

Ng, N.L., Herndon, S.C., Trimborn, A., Canagaratna, M.R., Croteau, P.L., Onasch, T.B. and Jayne, J.T. (2011). An Aerosol Chemical Speciation Monitor (ACSM) for Routine Monitoring of the Composition and Mass Concentrations of Ambient Aerosol. *Aerosol Sci. Technol.* 45: 780–794.

Pakkanen, T.A., Kerminen, V.M., Hillamo, R.E., Makinen, M., Makela, T. and Virkkula, A. (1996). Distribution of Nitrate over Sea-salt and Soil Derived Particles – Implications from a Field Study. *J. Atmos. Chem.* 24: 189–205.

Pathak, R.K., Wu, W.S. and Wang, T. (2009). Summertime $PM_{2.5}$ Ionic Species in Four Major Cities of China: Nitrate Formation in an Ammonia-deficient Atmosphere. *Atmos. Chem. Phys.* 9: 1711–1722.

Seinfeld, J.H. and Pandis, S.N. (2006). *Atmospheric Chemistry and Physics: From Air Pollution to Climate Change*, Second ed. John Willey & Sons, Inc., New York.

Shen, Z.X., Arimoto, R., Cao, J.J., Zhang, R.J., Li, X.X., Du, N., Okuda, T., Nakao, S. and Tanaka, S. (2008). Seasonal Variations and Evidence for the Effectiveness of Pollution Controls on Water-soluble Inorganic Species in Total Suspended Particulates and Fine Particulate Matter from Xi'an, China. *J. Air Waste Manage. Assoc.* 58: 1560–1570.

Sun, Y., Zhuang, G., Tang, A., Wang, Y. and An, Z. (2006). Chemical Characteristics of $PM_{2.5}$ and PM_{10} in Haze–fog Episodes in Beijing. *Environ. Sci. Technol.* 40: 3148–3155.

Sun, Y., Wang, Z., Dong, H., Yang, T., Li, J., Pan, X., Chen, P. and Jayne, J.T. (2012). Characterization of Summer Organic and Inorganic Aerosols in Beijing, China with an Aerosol Chemical Speciation Monitor. *Atmos. Environ.* 51: 250–259.

Sun, Y.L., Wang, Z., Fu, P., Jiang, Q., Yang, T., Li, J. and Ge, X. (2013). The Impact of Relative Humidity on Aerosol Composition and Evolution Processes during Wintertime in Beijing, China. *Atmos. Environ.* 77: 927–934.

Sun, Y., Jiang, Q., Wang, Z., Fu, P., Li, J., Yang, T. and Yin, Y. (2014). Investigation of the Sources and Evolution Processes of Severe Haze Pollution in Beijing in January 2013. *J. Geophys. Res.* 119, 4380–4398, doi: 10.1002/2014JD021641.

Tie, X.X., Wu, D. and Brasseur, G. (2009). Lung Cancer Mortality and Exposure to Atmospheric Aerosol Particles in Guangzhou, China. *Atmos. Environ.* 43: 2375–2377.

Turšič, J., Berner, A., Veber, M., Bizjak, M., Podkrajšek, B. and Grgić, I. (2003). Sulfate Formation on Synthetic Deposits under Haze Conditions. *Atmos. Environ.* 37: 3509–3516.

Wang, X., Wang, W., Yang, L., Gao, X., Nie, W., Yu, Y., Xu, P., Zhou Y. and Wang, Z. (2012). The Secondary Formation of Inorganic Aerosols in the Droplet Mode through Heterogeneous Aqueous Reactions under Haze Conditions. *Atmos. Environ.* 63: 68–76.

Wang, Y., Zhuang, G.S., Sun, Y.L. and Zheng, A. (2006). The Variation of Characteristics and Formation Mechanisms of Aerosols in Dust, Haze, and Clear Days in Beijing. *Atmos. Environ.* 40: 6579–6591.

Watson, J.G. (2002). Visibility: Science and Regulation. *J. Air Waste Manage. Assoc.* 52: 628–713.

Wu, D., Tie, X., Li, C., Ying, Z., Kai-Hon Lau, A., Huang, J., Deng, X. and Bi, X. (2005). An Extremely Low Visibility Event over the Guangzhou Region: A Case Study. *Atmos. Environ.* 39: 6568–6577.

Ye, X., Ma, Z., Zhang, J., Du, H., Chen, J., Chen, H., Yang, X., Gao, W. and Geng, F. (2011). Important Role of Ammonia on Haze Formation in Shanghai. *Environ. Res. Lett.* 6: 024019.

Zhang, Q., Streets, D.G., He, K., Wang, Y., Richter, A., Burrows, J.P., Uno, I., Jang, C.J., Chen, D., Yao, Z., and Lei, Y. (2007). NO_x Emission Trends for China, 1995-2004: The View from the Ground and the View from Space. *J. Geophys. Res.* 112: D22306, doi: 10.1029/2007 jd008684.

Zhang, R., Jing, J., Tao, J., Hsu, S.C., Wang, G., Cao, J., Lee, C.S.L., Zhu, L., Chen, Z. and Shen, Z. (2013). Chemical Characterization and Source Apportionment of $PM_{2.5}$ in Beijing: seasonal Perspective. *Atmos. Chem. Phys.* 13: 7053–7074.

Zhao, X.J., Zhao, P.S., Xu, J., Meng, W., Pu, W.W., Dong, F., He, D. and Shi, Q.F. (2013). Analysis of a Winter Regional Haze Event and Its Formation Mechanism in the North China Plain. *Atmos. Chem. Phys.* 13: 5685–5696.

Zhuang, H., Chan, C K., Fang, M. and Wexler, A.S. (1999). Formation of Nitrate and Non-sea-salt Sulfate on Coarse Particles. *Atmos. Environ.* 33: 4223–4233.

Received for review, December 23, 2014
Revised, February 2, 2015
Accepted, April 16, 2015